Int J Adv Manuf Technol (2012) 63:839–850
DOI 10.1007/s00170-012-3951-4

ORIGINAL ARTICLE

Modelling, simulation and experimental investigation of cutting forces during helical milling operations

Changyi Liu · Gui Wang · Matthew S. Dargusch

Received: 21 September 2011 / Accepted: 23 January 2012 / Published online: 18 February 2012

Abstract The kinematics of helical milling on a three-axis machine tool is first analysed. An analytical model dealing with time domain cutting forces is proposed in this paper. The cutting force model is established in order to accurately predict the cutting forces and torque during helical milling operations as a function of helical feed, spindle velocity, axial and radial cutting depth and milling tool geometry. The forces both on the side cutting edges and on the end cutting edges along the helical feed path are described by considering the tangential and the axial motion of the tool. The dual periodicity which is caused by the spindle rotation, as well as the period of the helical feed of the cutting tool, has been included. Both simulation and experiments have been performed in order to compare the results obtained from modelling with experiments.

Keywords Helical milling · Hole machining · Cutting forces · Analytical model · Time domain

Nomenclature

a_e^i, a_e^*	Radial cutting depth of side cutting edge and end cutting edge (millimetres)
a_p^i, a_p^*	Axial cutting depth of side cutting edge and end cutting edge (millimetres)
D_m	Milling tool diameter (millimetres)
F	Cutting force (newtons)
f_{va}	Axial component of helical feed speed (millimetres per second)
f_{vt}	X–Y plane component of helical feed speed (millimetres per second)
f_{za}	Axial component of helical feed rate per tooth (millimetres)
f_{zt}	X–Y plane component of helical feed rate per tooth (millimetres)
h^i, h^*	Instantaneous undeformed chip width of side cutting edge and end cutting edge (millimetres)
K_{rc}, K_{tc}, K_{ac}	Cutting force coefficients of radial, tangential and axial direction (newtons per square millimetre)
K_{re}, K_{te}, K_{ae}	Cutting force coefficients of edge effect (newtons per millimetre)
K^*_{vc}, K^*_{nc}	Tangential and normal cutting force coefficients of end cutting edges (newtons per square millimetre)
K^*_{ve}, K^*_{ne}	Tangential and normal cutting force coefficients of edge effect (newtons per millimetre)
P	Pitch of the helix feed trajectory
N_m	Flute number of the milling tool
v	Velocity of milling tool or velocity of a point of the cutting edge (millimetres per second)
t	Time (seconds)
β	Helix angle of the milling tool flute
θ	Angular of motive direction and X–Y plane of a point of the cutting edge (radians)
ϕ ϕ_j	Relative rotational angle of milling tool and the cutting tooth j (radians)
Φ_{st}, Φ_{ex}	Cut-in and cut-out relative rotational angle of the cutting tool
Φ_B	Diameter of the hole (millimetres)
Φ_O	Diameter of the helical feed trajectory in X–Y plane (millimetres)

C. Liu (✉)
Nanjing University of Aeronautics & Astronautics,
Nanjing, Jiangsu, China
e-mail: liuchangyi@nuaa.edu.cn

G. Wang · M. S. Dargusch
CAST CRC, School of Mechanical and Mining Engineering,
The University of Queensland,
Brisbane, Queensland, Australia

G. Wang
e-mail: gui.wang@uq.edu.au

M. S. Dargusch
e-mail: m.dargusch@cast.org.au

Ω	Spindle rotating angular velocity (radians per second)
Ω_h	Helix feed rotating angular velocity (radians per second)

1 Introduction

Helical milling has been applied to generate boreholes by means of a milling tool to some difficult-to-cut materials. This innovative method was found to facilitate hole making in AISI D2 tool steel in its hardened state, resulting in an enhancement in cutting tool life and the ability to machine H7 quality holes with a surface finish of 0.3 μm Ra [1]. The operation has also been applied to hole making in composite-metal compounds as a substitute for drilling operations. The impact of the axial and tangential feed per tooth on the process forces [2] has been investigated. Employing helical milling to aluminium with minimum quantity lubrication has shown an improvement in geometrical accuracy and a reduction in burr formation, lower cutting temperature and a smaller cutting force compared to drilling operations [3].

The prediction of cutting force through modelling and simulation is an important research area in order to improve process planning. Milling is the most complex machining operation. Previously in the literature, machining mechanisms have been derived from a general model [4, 5] and applied to the specific application, for example, five-axis milling, three-axis milling, peripheral milling, face milling and plunge milling. Modelling peripheral milling is a fundamental requirement in order to model more complex milling operations. A theoretical model based on the oblique cutting principle and cutting force coefficients has been developed in order to predict the cutting forces during peripheral milling [6–8]. Considering the helical flute (or side cutting edge) of the milling cutters, an attempt to accurately simulate milling forces including the effects of engaged flute length and the number of engaged flutes caused by the radial and axial depths of cut has been previously presented [9].

A common approach to facilitate the modelling of this complex situation including the milling tool geometry and the interaction with the workpiece involves analysing the cutting forces on axial discrete milling tools, then integrating these force elements. The intersection of the tool path swept envelope with the workpiece Z-buffer elements has been used to find the contact area between the cutter and the workpiece. An axial slice cutting tool discrete mechanistic model was used to estimate the cutting force vectors [10]. Cutter entry and exit angles, along with the immersion angles, were used as boundary conditions in order to predict cutting forces when flank milling ruled surfaces with tapered, helical and ball end mills [11]. The effect of lead and tilt angles between the cutter and the workpiece on the milling forces, tool deflections and form errors during multi-axis end milling have been analysed [12, 13].

During modelling of the cutting forces and system dynamics, one of the outstanding characteristics is that both side cutting edges and end cutting edges interact with the workpiece during helical milling processing. An accurate predictive model should describe and sum up the mechanics on both edges simultaneously. Ball end milling tools are most often used in three-axis or five-axis milling. Ball end milling tool processing models have been separated into ball end and cylindrical sections in order to obtain accurate prediction [10, 14, 15]. A mechanistic force model describing the cutting force as a sum of the cutting and edge forces has been developed for a general end milling cutter (cylindrical, taper, ball, bull nose) with the specific cutting and edge force coefficients identified [16].

As one type of three-axis milling operation, axial feed is a typical characteristic of helical milling operations. This operation uses a flat end mill not a ball end mill that is used in typical 3-axis and 5-axis milling situations. Axial feed using a flat end mill is also applied in plunge milling which is a two-axis operation. Considering rigid body motion of the cutter, the cutting force model and dynamics model for the plunge milling process in the time domain have been established [17, 18]. The cutting forces associated with plunge milling operations are predicted by considering the feed, radial engagement, tool geometry, spindle speed and the regeneration of the chip load due to vibrations [19]. Considering the flexibility of the workpiece, tool setting errors and tool kinematics and geometry, a horizontal approach was used to compute the chip area including the contribution of the main and side edge in the cutting zone [20].

Drilling operations and boring operations typically involve axial feed. Both these operations are similar to helical milling and plunge milling operations but with different cutting tools. The drilling cutting forces and dynamics have been integrated into the model in order to obtain drilled hole profiles [21]. A mechanistic model for predicting thrust force and torque during the drilling process using a drill tool with double-point angle edges [22]. To predict temperatures and forces on both the drilling and ball end milling operations, the cutting edges of the twist drill lip and the ball end mill were divided into oblique cutting elements [23]. A theoretical model to predict thrust and torque in high-speed drilling has been presented [24, 25]. The methodology for extracting cutting force coefficients for drilling operations has also been investigated [26]. When modelling the drilling process, the axial feed effect was not considered explicitly because the lip of the twist drill has a taper angle (point angle), and the interaction between the lip and workpiece caused by spindle rotation could lead to a spontaneous axial force (thrust).

In the literature, helical milling has been introduced as an enabling technology to substitute for drilling operations [1–3]. In recent years, research on modelling the mechanics of the helical milling process has been published [27, 28]. Although both the side cutting edges and the end cutting edges have been considered to participate in the machining process, the detail interaction between the end cutting edges and workpiece still needs more elaborate investigation and description.

Modelling, simulation and experimental investigation during cutting forces of the helical milling operation will be discussed in this paper including the influence of helical feed. This research aims to develop an analytical cutting force model in the time domain including both the axial cutting depth and the radial cutting depth associated with helical milling operations. The model considers the effects of both the tangential feed and axial feed, and the combination of both mechanics on the side cutting edges and the end cutting edges.

2 Kinematics of helical milling

In helical milling, the trajectory of a point on the milling tool cutting edge is the result of the spiral curve movement of the axis of the tool (reference frame) and the circular movement of the edge point relative to the axis (relative motion). Two sets of coordinates are defined to describe the motion of the cutter and the cutting force on the cutter; an X, Y, Z global coordinate frame fixed to the workpiece and an x, y, z local coordinate frame fixed to the cutting tool with the origin at the centre of the end flat surface which defines the reference frame. A description of helical milling with tool feed using helical trajectory and the coordinate settings are depicted in Fig. 1. The feed motion of the tool is decomposed into two components, f_{va} and f_{vt}.

$$f_{vt} = \frac{(\Phi_B - D_m)\Omega_h}{2} = \frac{N_m \Omega f_{zt}}{2\pi} (\text{mm/s}) \tag{1}$$

$$f_{va} = \frac{P\Omega_h}{2\pi} = \frac{N_m \Omega f_{za}}{2\pi} (\text{mm/s}) \tag{2}$$

The flat-end cylinder milling tools suitable for helical milling operations have two types of cutting edges: the side cutting edge (peripheral cutting edge) and the end cutting edge through the centre. The interaction characteristics of these two types with the workpiece are different. The side edges participate in the peripheral cutting component, while the end edges participate in the plunge cutting component. Therefore, these two movements will be initially analysed separately before being assembled or composed.

The side edge cutting process is typical intermittent cutting. The undeformed chip geometry, width, depth, and thickness have been described in the literature [2]. The side edge cutting process that is typical intermittent cutting is depicted in Fig. 2 (using superscript i). The velocity composition of an arbitrary point on the side cutting edge is described in cross section perpendicular to the tool axis. The undeformed chip geometry can be described as

$$a_e^i = \begin{cases} D_m, & \text{hole generating} \\ \frac{\Phi_B - \Phi_O}{2}, & \text{hole enlarging} \end{cases} \tag{3}$$

$$a_p^i(t) = \begin{cases} f_{va} t, & t \le 2\pi/\Omega_h \\ P, & t > 2\pi/\Omega_h \end{cases} \tag{4}$$

$$h^i = f_{zt} \sin\phi \tag{5}$$

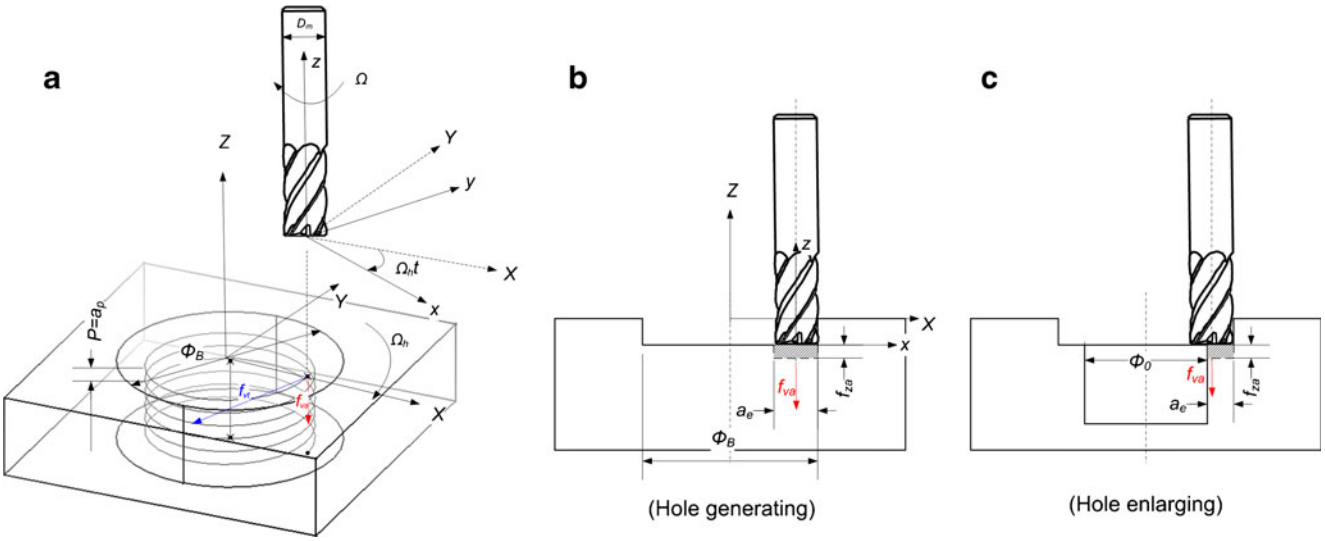

Fig. 1 Kinematics of helical milling

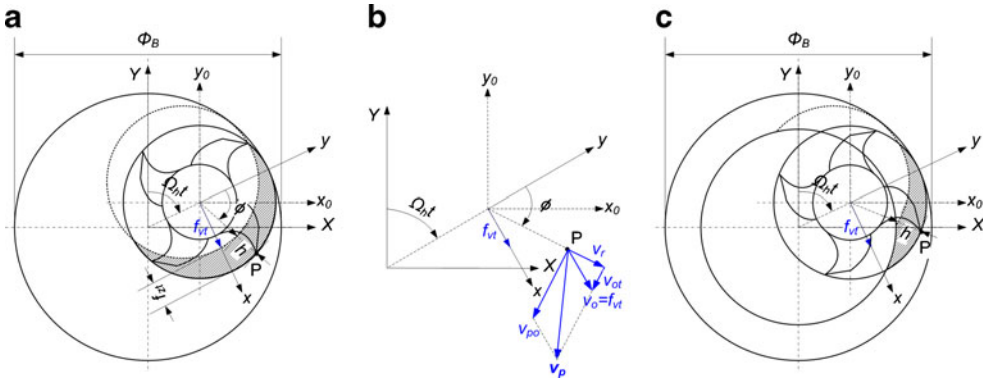

Fig. 2 Kinematics of the side cutting edge

where $\phi = 2\pi(\Omega \pm \Omega_h)t$ is the relative rotational angle of the cutter (+ up milling, − down milling).

The end edge cutting process, which is continuous cutting, is depicted in Fig. 3 (using superscript *). The velocity composition of an arbitrary point on the end cutting edge is described in the cross section perpendicular to the end cutting edge. The undeformed chip geometry, width and height can be described as:

$$a_e^* = \begin{cases} D_m, & \text{hole making} \\ \frac{\Phi_B - \Phi_O}{2}, & \text{hole enlarging} \end{cases} \tag{6}$$

$$h^* = f_{za}\cos\theta \tag{7}$$

3 Cutting force model for helical milling

3.1 Cutter feed influence on the cutting forces

The influence of cutter feed movement on the cutting forces during machining processing is almost always neglected. Similar to spindle rotation resulting in the relative movement between cutter and workpiece, cutter feed motion leads to relative movement also. This relative movement between the cutter and workpiece could influence the direction and magnitude of the cutting forces. The premise that the influence of the feed can be neglected is based on the assumption that the relative displacement and velocity from spindle rotation are much larger than the feed. Thus, in most situations, the influence of feed is insignificant and can be ignored.

However, when modelling some specific machining operations including axial feed, such as drilling, plunge milling and helical milling, to ignore the feed motion is unreasonable. If the axial feed effect is not considered, the cutting force along the axial direction might not be expressed accurately. For this reason, analysis of the influence of axial feed on cutting forces when modelling helical milling operations is necessary. In this paper, the feed motion effect on cutting forces has been analysed completely.

Firstly, the movement of an arbitrary point P at the side cutting edge could be decomposed to cylinder helical movement (reference movement) and circular movement perpendicular to the cutter axis, as depicted in Fig. 1. The reference movement can be decomposed to horizontal tangential feed and perpendicular axial feed, shown in Fig. 2. The horizontal velocity of point P is defined as $v_P = v_{PO} + v_O$, where v_O is identical to f_{vt}. For $\Omega >> \Omega_h$, means $|v_{PO}| >> |v_O|$, and therefore, $v_P \approx v_{PO}$. The influence of horizontal tangential feed on the side edge cutting force can be ignored.

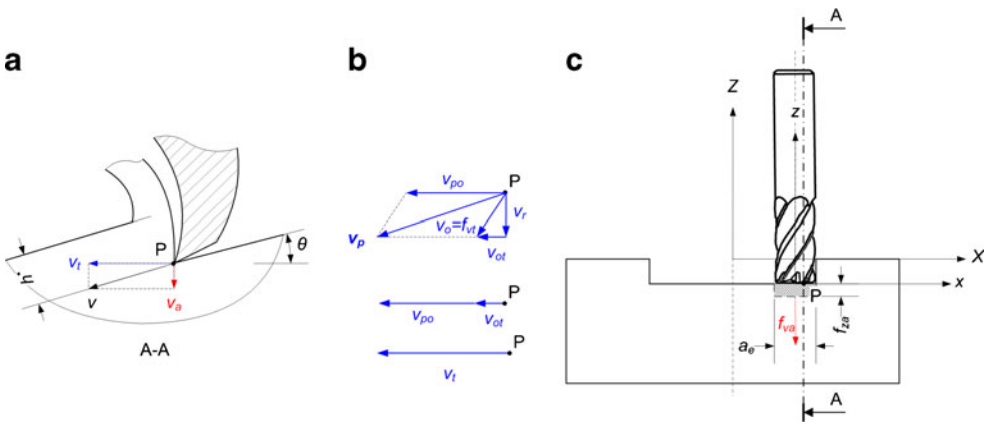

Fig. 3 Kinemics of the end cutting edge

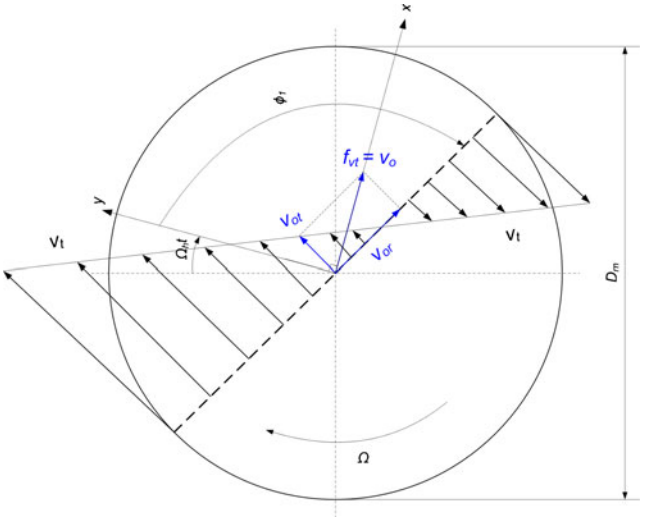

Fig. 4 Horizontal feed influence to forces on end cutting edges

Secondly, axial feed f_{vz} may result in a portion of the axial cutting force being on the side edge. For every axial feed, the cutting volume of the side edge is proportional to $f_{za}a_e h^i$, but the cutting volume of the end edge is proportional to $f_{za}a_e\pi(\Phi_B - D_m)/\sin\theta$. That means that the side edge undergoes intermittent cutting while the end edge undergoes continuous cutting. In the same time period, the cutting force derived from axial feed on the side edge is much smaller than that on the end side. So, the influence of axial feed on the side edge cutting force can also be ignored.

Then, assuming the top points on an end cutting edge in a straight line, the radial distance of point P to the cutting axis is variable. The influence of the horizontal feed f_{vt} is more outstanding when P is near to the axis. The horizontal movement of point P at the end edge can be decomposed into the relative tangential part v_t and relative radial part v_r, as described in Fig. 3. Compared to drilling or plunge milling operations in which tangential cutting forces are vanished and tangential velocity of the z-axis is zero, tangential forces and axis tangential velocity of the helical milling are not zero, as depicted in Fig. 4. For the aforementioned reason, the influence of horizontal tangential feed on end edge cutting forces can be ignored.

The existence of the relative radial part v_r of the end edge implies that the radial force also exists. If we consider the end cutting edge of the flat-end milling cutter as approximately a straight line, the cutting edge along the radial direction slides rather than shears. F_r^* should be the friction force that is smaller than the shear force. Therefore, the radial force on the end edge can be neglected, or $F_a^* = 0$.

Finally, due to the axial feed associated with f_{va}, the displacement direction of the end edge is not horizontal but having an angle θ relative to f_{va} and f_{vz}. After calculating this angle, the actual direction of the machined surface, the variation of the rake angle and the clearance angle can be defined. The cutting force on the end edge derived from axial feed can be defined within the plane to which the machined surface belongs.

3.2 Side cutting edge

Based on the kinematics of the helical milling process, two new features that may influence the cutting force and dynamics of the helical milling process have been considered. One was the periodic force variation created by the circular or tangential feed of the tool, and the other is the additional force component generated by the axial feed of the tools. The axial feed force mostly occurs at the end cutting edge of the milling tools. The interaction conditions between the tool and the workpiece are the combination of side edge cutting forces and end edge cutting forces.

$$\overrightarrow{F} = \overrightarrow{F}^{i} + \overrightarrow{F}^{*} \tag{8}$$

Where, $\overrightarrow{F}^{i}$ is the side cutting edge component and $\overrightarrow{F}^{*}$ is end cutting edge component. Considering a point **P** on the (jth)

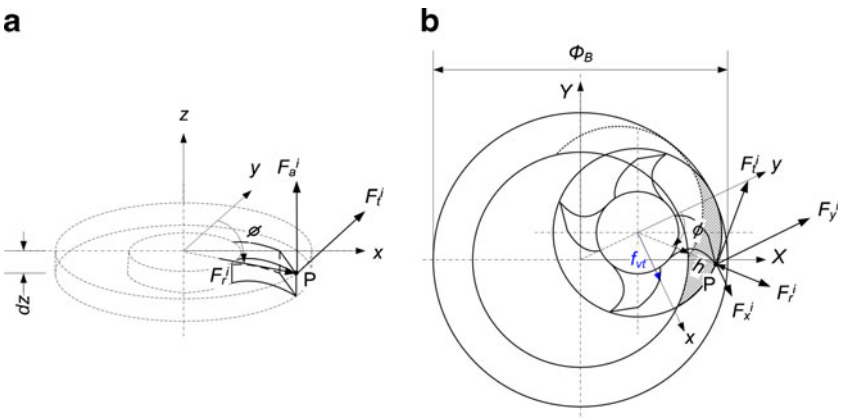

Fig. 5 Cutting forces on the side cutting edge

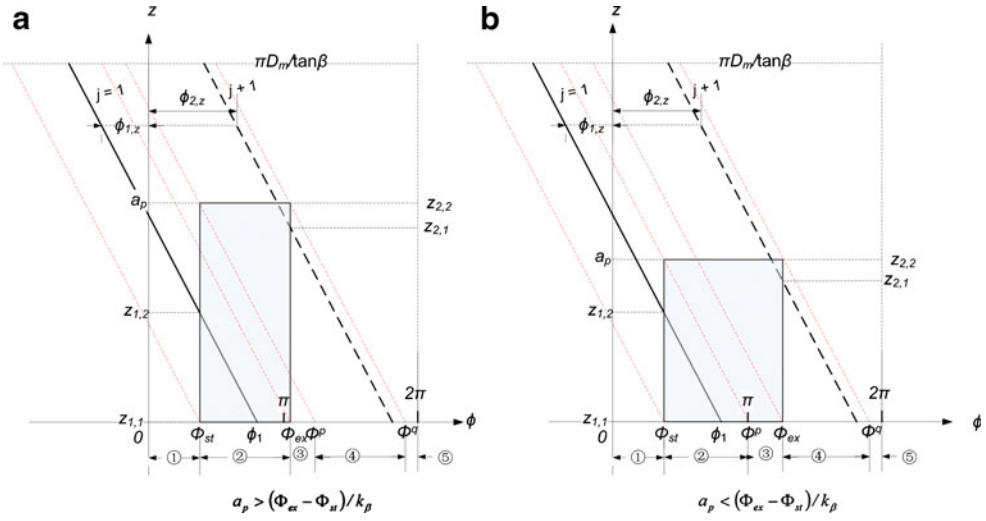

Fig. 6 Different intervals of a cutting period. **a** $a_p > (\Phi_{ex} - \Phi_{st})/k_\beta$, **b** $a_p < (\Phi_{ex} - \Phi_{st})/k_\beta$

cutting tooth, shown in Fig. 5, the integration cutting force $\overrightarrow{F}^i$ (defined in the local coordinate system) along the in-cut portion of the flute j is similar to that presented in the referenced literature [4].

$$F^i_{x,j}(\phi_j(z)) = \left\{ \frac{f_{zt}}{4k_\beta}\left[-K_{tc}\cos 2\phi_j(z) + K_{rc}\left(2\phi_j(z) - \sin 2\phi_j(z)\right)\right] + \frac{1}{k_\beta}\left[K_{te}\sin\phi_j(z) - K_{re}\cos\phi_j(z)\right] \right\}_{\phi_{j,z}(z_{j,1})}^{\phi_{j,z}(z_{j,1})} \tag{9}$$

$$F^i_{y,j}(\phi_j(z)) = \left\{ \frac{-f_{zt}}{4k_\beta}\left[K_{tc}\left(2\phi_j(z) - \sin 2\phi_j(z)\right) + K_{rc}\cos 2\phi_j(z)\right] + \frac{1}{k_\beta}\left[K_{te}\cos\phi_j(z) + K_{re}\sin\phi_j(z)\right] \right\}_{\phi_{j,z}(z_{j,1})}^{\phi_{j,z}(z_{j,1})} \tag{10}$$

$$F^i_{z,j}(\phi_j(z)) = \frac{1}{k_\beta}\left[K_{ac} f_{zt}\cos\phi_j(z) + K_{ae}\phi_j(z)\right]_{\phi_{j,z}(z_{j,1})}^{\phi_{j,z}(z_{j,1})} \tag{11}$$

where $k_\beta = 2\tan\beta/D_m$

The detail of the integration of these forces is complicated because the contours of the side edge of the generic milling cutter are helical circles. To get the details of the forces at an arbitrary time, the integration procedure at one period (e.g. from zero to 2π) of the forces on the discrete cutter has to be

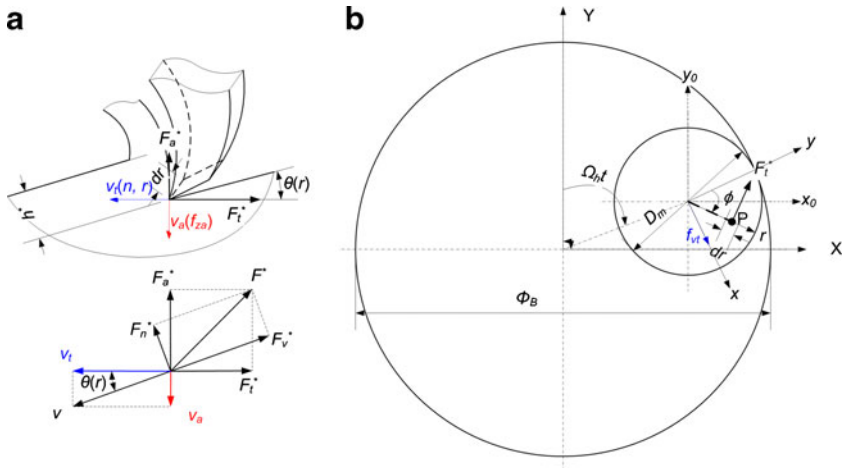

Fig. 7 Cutting forces on the end cutting edge

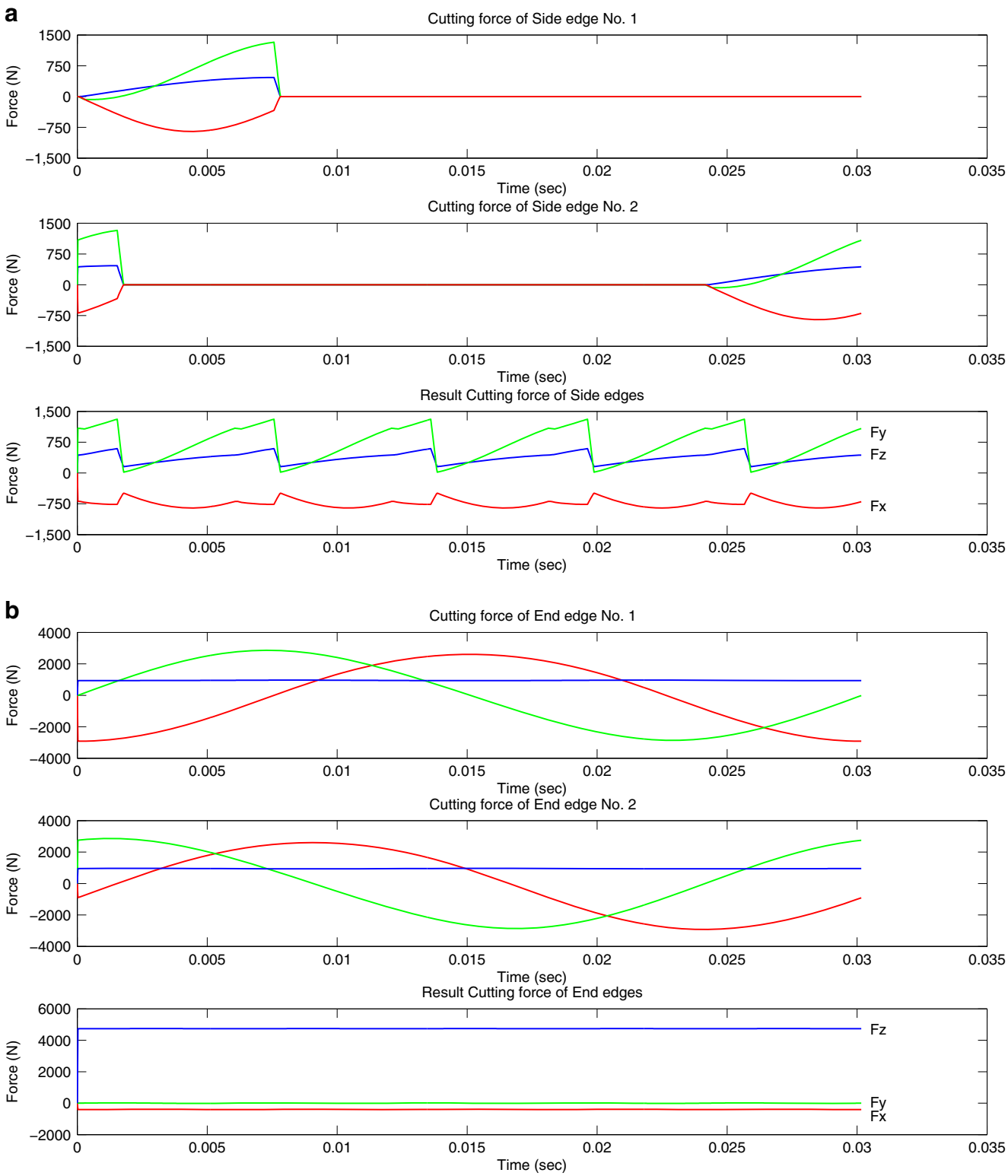

Fig. 8 Simulation of the cutting forces during helical milling (milling tool diameter D_m 16 mm, five flutes, cutting speed v_c 100 m/min, axial feed rate per tooth f_{za} 0.2 mm, tangential feed rate per tooth f_{zt} 0.5 mm, radial cutting depth a_e 8 mm, up milling)

divided into several time intervals, as shown in Fig. 6. The oblique lines represent the unfolding of the milling tool flutes in a plane.

If $a_p > (\Phi_{ex} - \Phi_{st})/k_\beta$ is as shown in Fig. 6a, axial cutting depth is large. Φ_{st} and Φ_{ex} is the cut-in and cut-out relative rotational angle of the cutter, respectively.

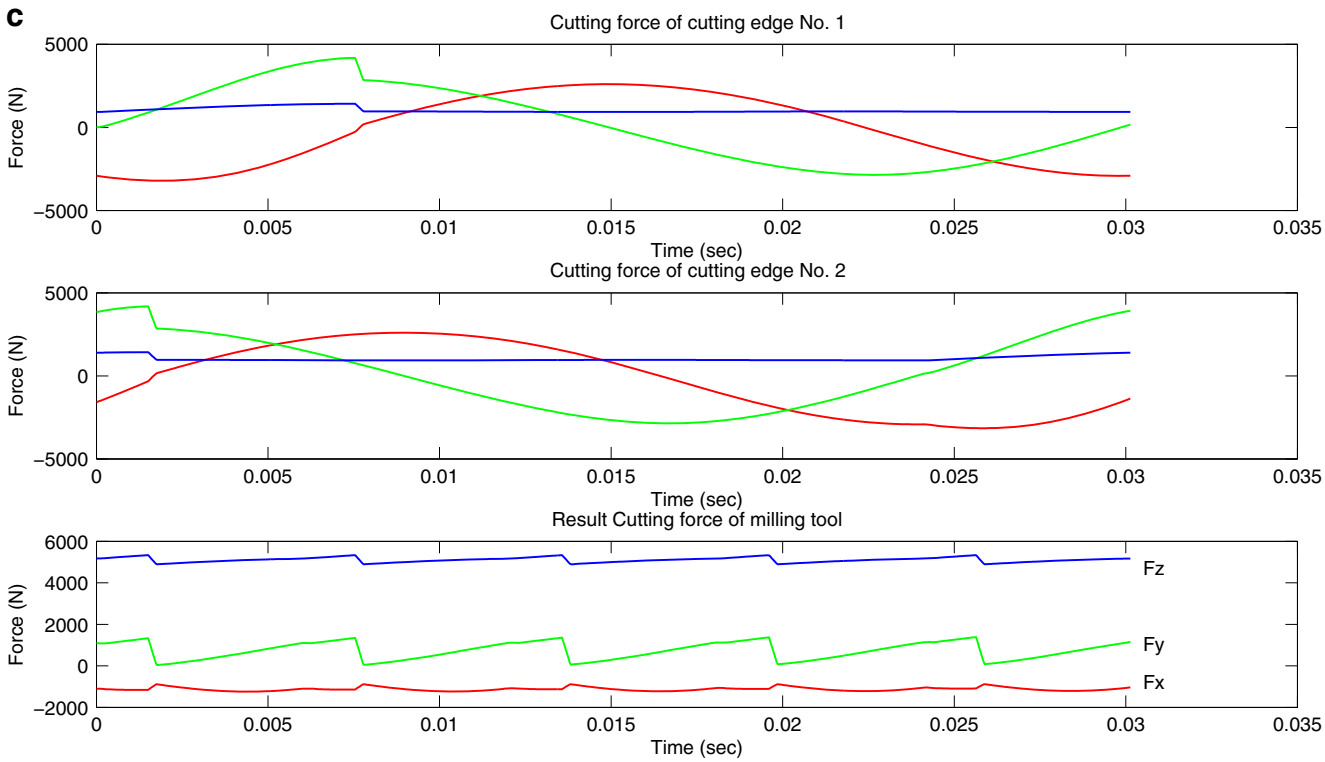

Fig. 8 (continued)

In intervals 1 and 5, there are no interactions between the cutter and workpiece, and therefore, the cutting force $0 \le \phi_j < \Phi_{st}, \overrightarrow{F}_j = 0; \Phi^q \le \phi_j < 2\pi, \overrightarrow{F}_j = 0$

During interval 2, the cutting tooth begins to cut into the workpiece, where $\Phi_{st} \le \phi_j < \Phi_{ex}, \phi_j(z_1) = \phi_j, \phi_j(z_2) = \Phi_{st}$

During interval 3, the cutting tooth is fully involved in cutting the workpiece until the maximum axial cutting depth a_p, where $\Phi_{ex} \le \phi_j < \Phi^p, \phi_j(z_1) = \Phi_{ex}, \phi_j(z_2) = \Phi_{st}$ is obtained.

During interval 4, the cutting tooth completes the cutting and quits the interaction finally, where $\Phi^p \le \phi_j < \Phi^q, \phi_j(z_1) = \Phi_{ex}, \phi_j(z_2) = \phi_j - (\Phi^p - \Phi_{st})$

If $a_p < (\Phi_{ex} - \Phi_{st})/k_\beta$ as shown in Fig. 6b, axial cutting depth is large.

In interval 1 and 5, there is no interaction between the cutter and workpiece, and therefore no cutting force. $0 \le \phi_j < \Phi_{st}, \overrightarrow{F}_j = 0; \Phi^q \le \phi_j < 2\pi, \overrightarrow{F}_j = 0$

During interval 2, the cutting tooth begins to cut into the workpiece and progress towards the maximum axial cutting depth a_p, where $\Phi_{st} \le \phi_j < \Phi^p, \phi_j(z_1) = \phi_j, \phi_j(z_2) = \Phi_{st}$

During interval 3, the cutting tooth interacts with the workpiece with a_p, where $\Phi^p \le \phi_j < \Phi_{ex}, \phi_j(z_1) = \phi_j, \phi_j(z_2) = \phi_j - (\Phi^p - \Phi_{st})$

During interval 4, the cutting tooth completes the cutting operation and quits the interaction finally, where $\Phi_{ex} \le \phi_j < \Phi^q, \phi_j(z_1) = \Phi_{ex}, \phi_j(z_2) = \phi_j - (\Phi^p - \Phi_{st})$

3.3 End cutting edge

Since both the tangential feed f_{vt} and axial feed f_{va} are present during helical milling, the end cutting edge force component and the edge of these teeth are assumed to be a straight line and coincide with the radial line during analysis. If the friction force is neglected along the end cutting edge, the radial force $F_a^* = 0$. As shown in Fig. 7, the end cutting edge force component can be represented as

$$dF_v^* = K_{vc}^* f_{za} \cos\theta dr + K_{ve}^* dr \tag{12}$$

$$dF_n^* = K_{nc}^* f_{za} \cos\theta dr + K_{ne}^* dr \tag{13}$$

$$dF_t^* = dF_v^* \cos\theta - dF_n^* \sin\theta \tag{14}$$

$$dF_a^* = dF_v^* \sin\theta + dF_n^* \cos\theta \tag{15}$$

$$dT^* = r dF_t^* \tag{16}$$

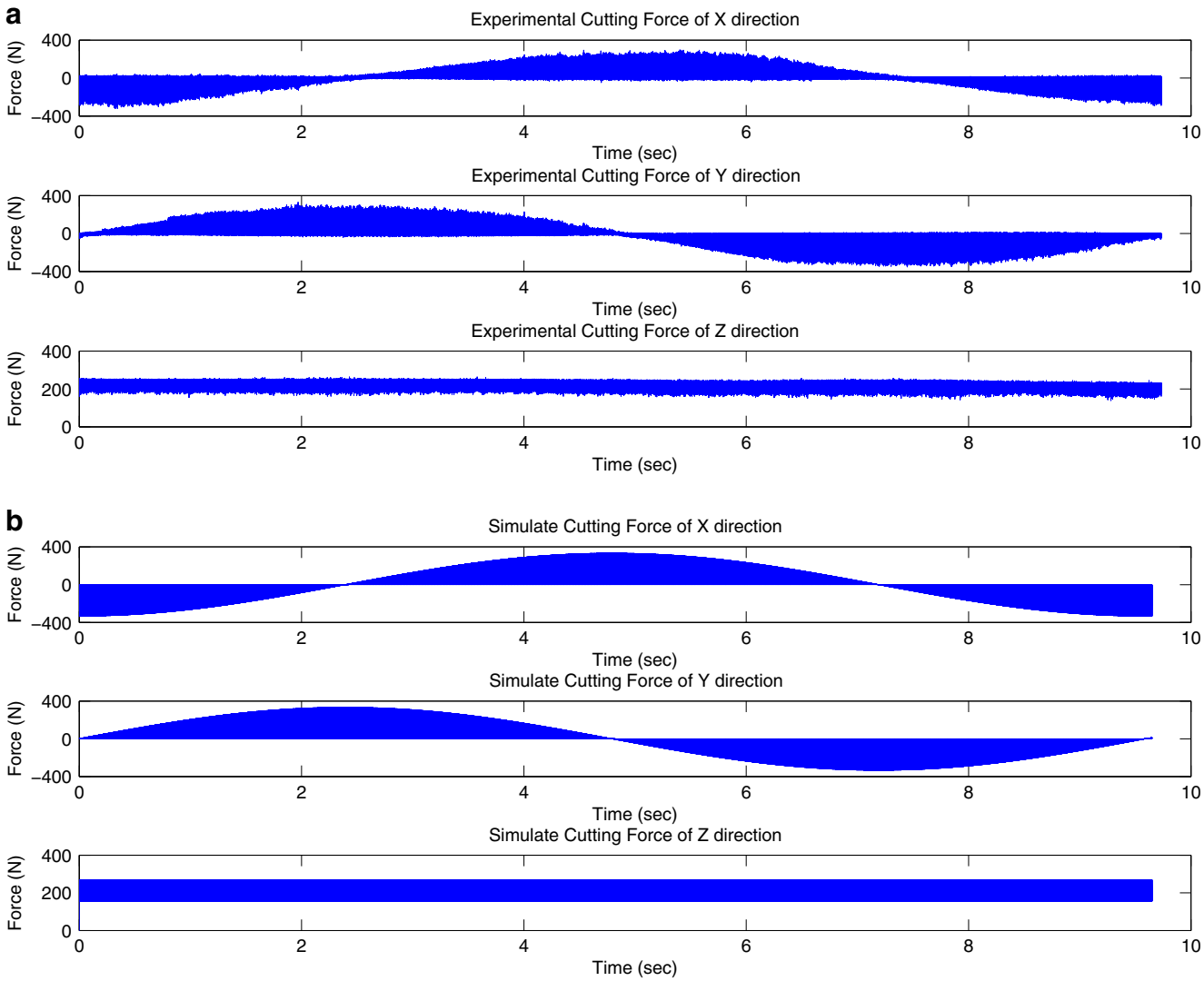

Fig. 9 Cutting force result from experiment and simulation during helical milling cutting (milling tool M.A. Ford 20-mm five-flute end mill 17878703A, cutting speed v_c 100 m/min, axial feed rate per tooth f_{za} 0.005 mm, tangential feed rate per tooth f_{zt} 0.1 mm, radial cutting depth a_e 1 mm, down milling)

$$\text{Denote } A = \frac{N_m f_{za}}{2\pi}, B = \frac{N_m f_{zt}\cos\phi_j}{2\pi}, \theta = \arctan\frac{v_a}{v_t} = \arctan\frac{A}{r+B},$$

$$[\Theta] = \int_{\frac{D_m}{2}-a_e^*}^{\frac{D_m}{2}} \mathrm{d}r \begin{bmatrix} \cos\theta & -\sin\theta & 0 \\ \sin\theta & \cos\theta & 0 \\ 0 & 0 & 0 \\ r\cos\theta & -r\sin\theta & 0 \end{bmatrix},$$

$$[K^*] = \begin{bmatrix} K_{vc}^* & K_{ve}^* \\ K_{nc}^* & K_{ne}^* \\ K_{rc}^* & K_{re}^* \end{bmatrix}, \text{ therefore,}$$

$$\begin{Bmatrix} F_{t,j}^* \\ F_{a,j}^* \\ F_{r,j}^* \\ T_j^* \end{Bmatrix} = [\Theta][K^*] \begin{Bmatrix} f_{za} \\ 1 \end{Bmatrix} \tag{17}$$

Transform to the local coordinate,

$$\begin{Bmatrix} F_{x,j}^* \\ F_{y,j}^* \\ F_{z,j}^* \\ T_j^* \end{Bmatrix} = \begin{Bmatrix} -F_{t,j}^* \cos\left(\phi_j(t)\right) \\ F_{t,j}^* \sin\left(\phi_j(t)\right) \\ F_{a,j}^* \\ T_j^* \end{Bmatrix} \tag{18}$$

Sum up side cutting edge forces and end cutting forces on the jth tooth and convert to global coordinates.

$$\begin{Bmatrix} F_{x,j} \\ F_{Y,j} \\ F_{Z,j} \\ T_{Z,j} \end{Bmatrix} = \begin{bmatrix} \cos\Omega_h t & \sin\Omega_h t & 0 & 0 \\ -\sin\Omega_h t & \cos\Omega_h t & 0 & 0 \\ 0 & 0 & 1 & 0 \\ 0 & 0 & 0 & 1 \end{bmatrix} \begin{Bmatrix} F_{x,j}^i + F_{x,j}^* \\ F_{y,j}^i + F_{y,j}^* \\ F_{z,j}^i + F_{z,j}^* \\ T_j^* \end{Bmatrix} \tag{19}$$

Then, sum up all the cutting forces on the cutting teeth to obtain the cutting force model.

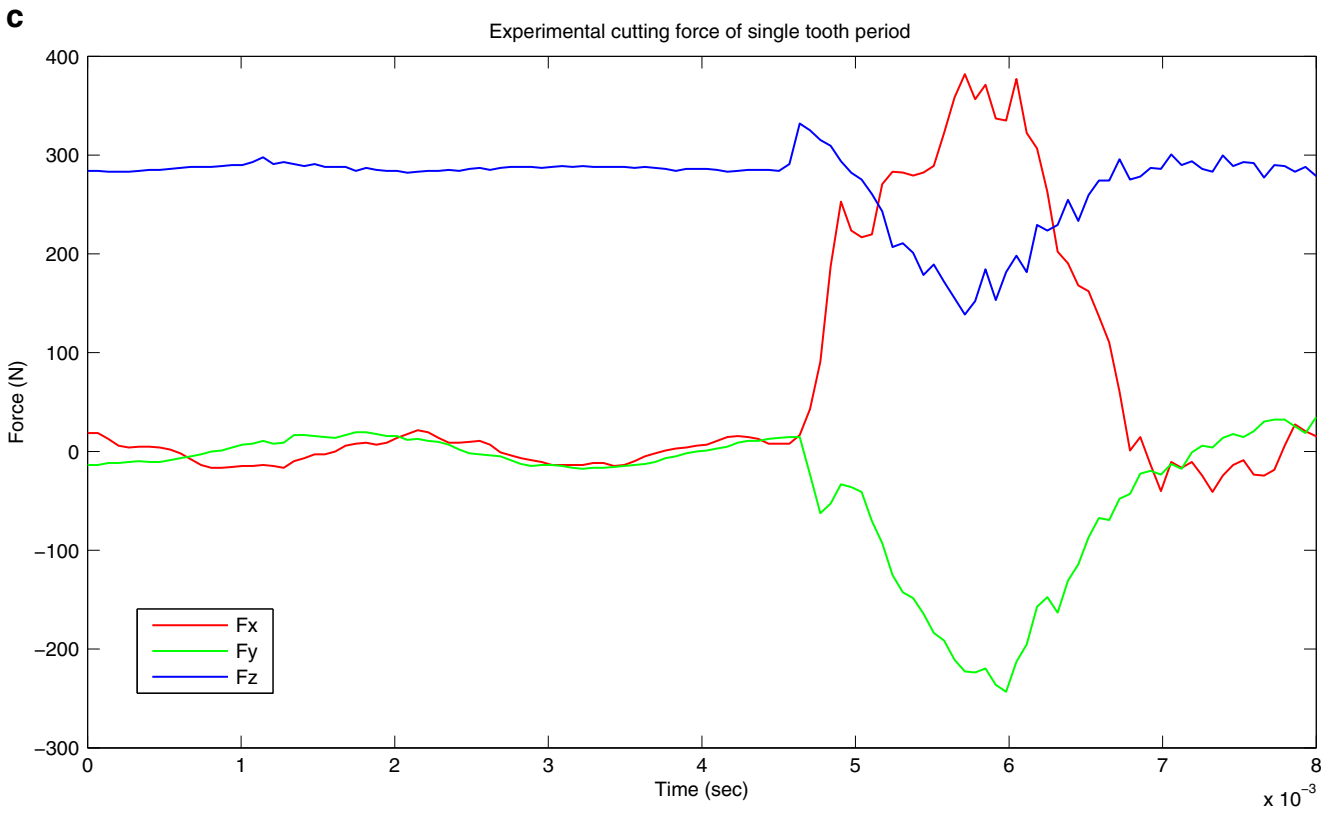

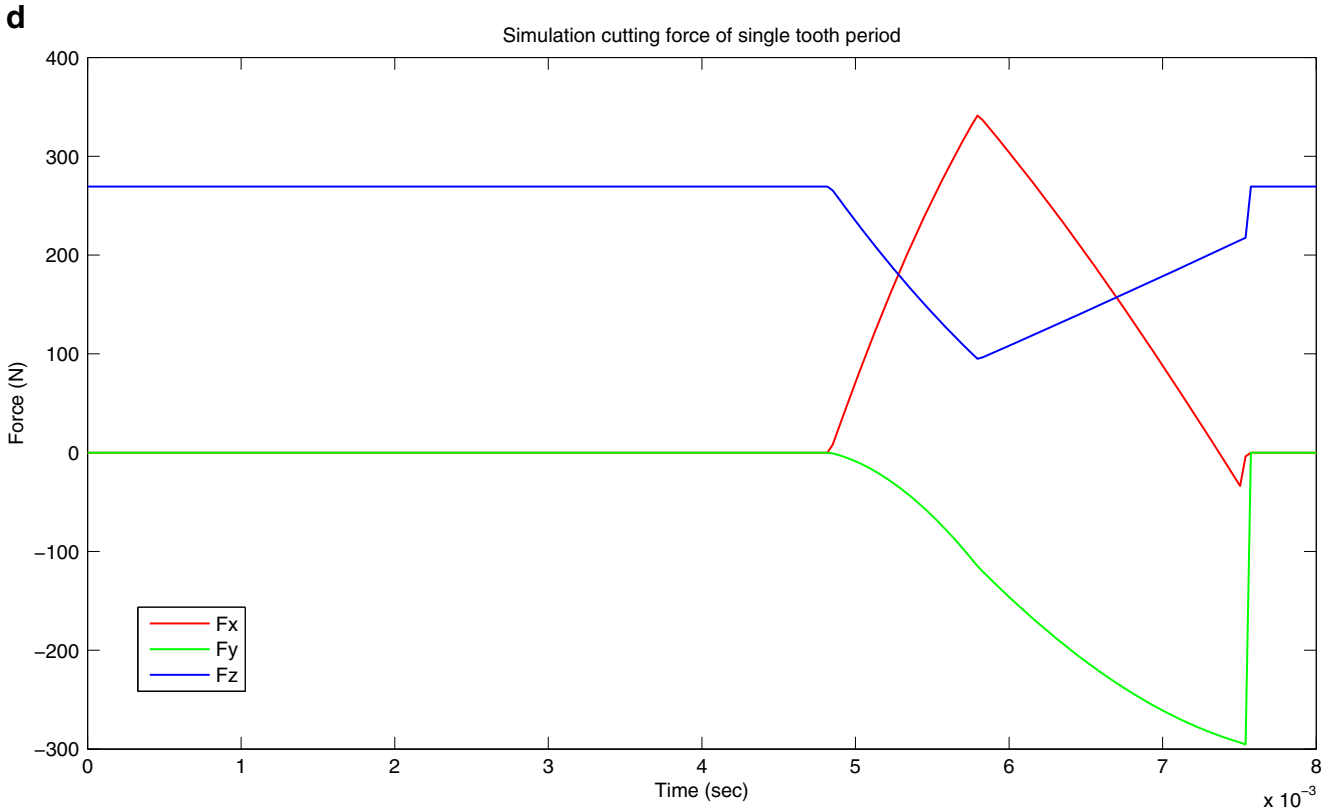

Fig. 9 (continued)

$$\begin{Bmatrix} F_X \\ F_Y \\ F_Z \\ T_Z \end{Bmatrix} = \sum_{j=1}^{N_m} \begin{Bmatrix} F_{Xj}\left(\Omega t + (j-1)\frac{2\pi}{N}\right) \\ F_{Yj}\left(\Omega t + (j-1)\frac{2\pi}{N}\right) \\ F_{Zj}\left(\Omega t + (j-1)\frac{2\pi}{N}\right) \\ T_{Zj}\left(\Omega t + (j-1)\frac{2\pi}{N}\right) \end{Bmatrix} \quad (20)$$

The cutting force model during helical milling operations in the time domain has therefore been established analytically. This model defines both the cutting force on the side cutting edge and on the end cutting edge, incorporating the interactions between the cutter and the workpiece on the effect of the spindle rotation and the helical feed.

4 Simulations and experimental results

Cutting forces during helical milling have been simulated on the MATLAB platform using the models presented previously, and experiments have been performed to compare with the model predictions. The process parameters included the workpiece material, cutting conditions, tool material and geometry. The Ti6Al4V alloy was cast and then HIPed (hot isostatic pressing, HIP) at a pressure of 100–140 MPa at 920°C for 2.5 h; then, the casting was rough milled to the end geometry (160×160×20 mm) with a hole in a diameter of 60 mm in the centre of the plate as shown in Fig. 1. There were two types of cutting tools, the M.A. Ford 20-mm five-flute carbide end mill (17878703A) and the M.A. Ford 16-mm five-flute carbide end mill (17862903A).

Experiments were carried out on a five-axis high-speed Mikron UCP-710 CNC machining centre. A three-axis piezo-electric Kistler 9265B type dynamometer was set up on the fixture with the workpiece. The accessory data acquisition system of the dynamometer consisted of a Kistler 5019A type multi-channel charge amplifier and signal processing software DynoWare. Before commencing the experiments, the dynamometer was calibrated using static loads.

The simulated cutting forces in an entire milling tool revolution on the side edges, end edges and whole cutter during the typical cutting conditions are depicted in Fig. 8. In this simulation, the up milling and large radial cutting depth are considered as the significant characteristics of the operation. Figure 8a shows the simulated cutting forces that acted on first side cutting edge, second side cutting edge and cutting forces that acted on the milling tool from both the five cutting edges, respectively. For the up milling condition, the *j*th edge engages with the workpiece, and the (*j*-1)th edge engages following. The large radial cutting depth means that before the previous cutting edge has completed cutting, the next cutting edge has engaged the workpiece. Therefore, there is a period of time that forces overlap between the consecutive cutting edges. Figure 8b shows the simulated cutting forces that acted on the end cutting edges. There are similar cutting forces superposing between consecutive side cutting edges. However, the sum of the *X*, *Y* direction forces are nearly zero, that is one of the important features of helical milling and plunge milling operations. Figure 8c shows the cutting forces that acted on the milling tool. These results are the integration of the component forces from Fig. 8a and b.

The simulated and experimental cutting force results are compared in Fig. 9. In this case, cutting tools travel along an entire helical curve and machine an entire helical milling period. The *X*, *Y*, *Z* coordinates are fixed to the workpiece, during the helical feed motion of the tool, the amplitude of F_X and F_Y change with time following a sine relationship. The amplitude of Fig. 9a and b counter profile is the maximum result of F_X and F_Y. Figure 9c and d shows the experimental and simulated cutting forces in detail in a single tooth period.

The comparison result from experiment and simulation are shown in Table 1. This figure depicts the simulation results to an accuracy of about 10% in these selected indicators. The maximum value of F_X, F_Y and F_Z indicates for a single tooth period for both simulation and experimental results shown. The maximum of $\sqrt{F_X^2 + F_Y^2}$ indicates the amplitude of force of F_X and F_Y during helical milling. The errors probably result from cutting tool deflection and cutting tool wear.

5 Conclusion

In this paper, cutting forces during helical milling operations have been modelled in the time domain. The cutting forces both on the side cutting edges and on the end cutting edges along the helical feed path have been modelled by considering the tangential and the axial motion of the tool. The cutting force model can be used to predict cutting forces both on the side cutting edges and the end cutting edges. The model can also predict forces on the whole helix milling tool considering the process parameters and tool geometry. The experimental results show that for the given helix milling operation parameters, the result of simulation predicts the cutting forces effectively and accurately.

Table 1 Comparison of experiment and simulation results

	Experiment (average)	Simulation	Error
Helical feed period (s)	9.50	9.475	0.263%
Maximum of F_X (N)	371.1	341.2	−8.06%
Maximum of F_Y (N)	253.2	283.2	11.8%
Maximum of F_Z (N)	287.7	269.4	−6.36%
Maximum of $\sqrt{F_X^2 + F_Y^2}$ (N)	365.3	397.6	8.84%

References

1. Iyer R, Koshy P, Ng E (2007) Helical milling: an enabling technology for hard machining precision holes in AISI D2 tool steel. Int J Mach Tool Manuf 47(2):205–210
2. Denkena B, Boehnke D, Dege JH (2008) Helical milling of CFRP—titanium layer compounds. CIRP J Manuf Sci Tech 1(2):64–69
3. Sasahara H, Kawasaki M, Tsutsumi M (2003) Helical feed milling with MQL for boring of aluminum alloy. Trans Jpn Soc Mech Eng C 69(8):2156–2161. doi:10.1299/kikaic.69.2156
4. Altintas Y (2000) Manufacturing automation: principles of metal cutting and machine tool vibrations. New York, Cambridge
5. Altintas Y, Engin S (2001) Generalized modeling of mechanics and dynamics of milling cutters. CIRP Ann Manuf Technol 50 (1):25–30
6. Liu XW, Cheng K, Webb D, Luo XC (2002) Improved dynamic cutting force model in peripheral milling. Part I: theoretical model and simulation. Int J Adv Manuf Technol 20(9):631–638
7. Liu XW, Cheng K, Webb D, Longstaff AP, Widiyarto MH (2004) Improved dynamic cutting force model in peripheral milling. Part II: experimental verification and prediction. Int J Adv Manuf Technol 24(11–12):794–805
8. Li HZ, Zhang WB, Li XP (2001) Modelling of cutting forces in helical end milling using a predictive machining theory. Int J Mech Sci 43(8):1711–1730
9. Lai W, Greenway B, Faddis T (2001) Flute engagement in peripheral milling. J Mater Process Technol 117(1–2):1–8
10. Fussell BK, Jerard RB, Hemmett JG (2003) Modeling of cutting geometry and forces for 5-axis sculptured surface machining. CAD Comput Aided Des 35(4):333–346
11. Larue A, Altintas Y (2005) Simulation of flank milling processes. Int J Mach Tool Manuf 45(4–5):549–559
12. Wei ZC, Wang MJ, Han XG (2010) Cutting forces prediction in generalized pocket machining. Int J Mach Tool Manuf 50(5–8):449–458
13. Lazoglu I, Liang SY (2000) Modeling of ball-end milling forces with cutter axis inclination. J Manuf Sci Eng Trans ASME 122(1):3–11
14. Budak E, Ozturk E, Tunc LT (2009) Modeling and simulation of 5-axis milling processes. CIRP Ann Manuf Technol 58(1):347–350
15. Ozturk E, Budak E (2010) Dynamics and stability of five-axis ball-end milling. J Manuf Sci Eng Trans ASME 132(2). doi:10.1115/1.4001038
16. Gradisek J, Kalveram M, Weinert K (2004) Mechanistic identification of specific force coefficients for a general end mill. Int J Mach Tool Manuf 44(4):401–414
17. Ko JH, Altintas Y (2007) Dynamics and stability of plunge milling operations. J Manuf Sci Eng Trans ASME 129(1):32–40
18. Altintas Y, Ko JH (2006) Chatter stability of plunge milling. CIRP Ann Manuf Technol 55(1):361–364
19. Ko JH, Altintas Y (2007) Time domain model of plunge milling operation. Int J Mach Tool Manuf 47(9):1351–1361
20. Damir A, Ng EG, Elbestawi M (2011) Force prediction and stability analysis of plunge milling of systems with rigid and flexible workpiece. Int J Adv Manuf Technol 54(9–12):853–877
21. Pirtini M, Lazoglu I (2005) Forces and hole quality in drilling. Int J Mach Tool Manuf 45(11):1271–1281
22. de Lacalle LNL, Rivero A, Lamikiz A (2009) Mechanistic model for drills with double point-angle edges. Int J Adv Manuf Technol 40(5–6):447–457
23. Shatla M, Altan T (2000) Analytical modeling of drilling and ball end milling. J Mater Process Technol 98(1):125–133
24. Elhachimi M, Torbaty S, Joyot P (1999) Mechanical modelling of high speed drilling. 1: Predicting torque and thrust. Int J Mach Tool Manuf 39(4):553–568
25. Elhachimi M, Torbaty S, Joyot P (1999) Mechanical modelling of high speed drilling. 2: Predicted and experimental results. Int J Mach Tool Manuf 39(4):569–581
26. Hamade RF, Seif CY, Ismail F (2006) Extracting cutting force coefficients from drilling experiments. Int J Mach Tool Manuf 46 (3–4):387–396
27. Li Z, Liu Q, Peng C, Sun X (2010) Cutting force modeling and simulation for hole-making operation by helical milling. Proc SPIE 7997:799703. doi:10.1117/12.883034
28. Wang H, Qin X, Ren C, Wang Q (2011) Prediction of cutting forces in helical milling process. Int J Adv Manuf Technol. doi:10.1007/s00170-011-3435-y